
# Evolution of surface grain structure and mechanical properties in orthogonal cutting of titanium alloy



| | |
|---|---|
| Journal: | *Journal of Materials Research* |
| Manuscript ID | JMR-2016-0747 |
| Manuscript Type: | Metallic Materials Article |
| Date Submitted by the Author: | 03-Aug-2016 |
| Complete List of Authors: | Bai, Jinxuan; Harbin Institute of Technology, School of Mechanical and Electrical Engineering<br>Bai, qingshun; Harbin Institute of Technology, School of Mechanical and Electrical Engineering<br>Tong, Zhen; Harbin Institute of Technology, School of Mechanical and Electrical Engineering; University of Huddersfield, Centre for Precision Technologies<br>Hu, Chao; Harbin Institute of Technology, School of Mechanical and Electrical Engineering<br>He, xin; Harbin Institute of Technology, School of Mechanical and Electrical Engineering |
| Key Words: | dislocations, microstructure, grain size |
| | |

# Evolution of surface grain structure and mechanical properties in orthogonal cutting of titanium alloy

Jinxuan Bai[1*], Qingshun Bai[1], Zhen Tong[1,2], Chao Hu[1], Xin He[1]

*1 School of Mechanical and Electrical Engineering, Harbin Institute of Technology, Harbin 150001, China*

*2 Centre for precision Technologies, University of Huddersfield, Huddersfield HD1 3DH, UK*

**Corresponding author:* jinxuanbai@hit.edu.cn

**Abstract**: In this study, a mesoscale dislocation simulation method was developed to study the orthogonal cutting of Titanium alloy. The evolution of the surface grain structure and its effects on the mechanical properties was studied using two-dimensional climb assisted dislocation dynamic technology. The motions of edge dislocations in an elastic matrix such as dislocation nucleation, lock, interaction with obstacles and grain boundaries, and annihilation were tracked. The results showed that the machined surface has a graded microstructure composed of ultrafine grains. A grain refinement process was observed in micro-cutting of titanium alloy. The process can be described as follows: (i) the development of dislocation lines in original grains, (ii) the formation of dense dislocation bands, (iii) the transformation of dislocation bands into subgrain boundaries, and (iv) the continuous dynamic recrystallization in subgrain boundaries. The fine-grains formed in this process bring appreciable scale effect and a mass of dislocations pile up in the grain boundary and persistent slip band (PSB). In particular, the flow stress and hardening rate was reduced by dislocation climb. However, this effect is significantly weakened when grain size was less than 1.65 μm. In addition, a Hall-Petch type relation is predicted depending on the amount of slips, the dislocation density, the grain arrangement and the range of grain sizes to which a Hall-Petch expression is fit. The numerical results obtained were compared with experimental data gathered from literature and a satisfied agreement was found.

**Keywords**: Titanium alloy; plastic behavior; multi-scale simulation; dislocation dynamic; grain refinement



## 1. Introduction

The use of titanium and its alloys in aerospace industry has increased recently because of their superior properties and improvements in machinability of these alloys [1]. Ultra-precision manufacturing (UPM) technology is one of the most important methods to produce high-quality titanium alloy components with surface precision and roughness in nanometer range [2]. However, during ultra-precision cutting, the titanium alloy specimens suffer from a combination of various deformations, which reduce machining precision and surface roughness. In addition, microstructure near the machined surface of component can be significantly changed by the material removal process, which can affect the functional performance of the components. In-depth understanding of the mechanism of material removal, especially knowing the dynamics characteristics of workpiece and the main factors affecting surface integrity can provide an effective way to improve the machining precision. Although numerous previous studies can be found in literature reporting the formation of hardened layer on the machined surface, the prediction of material characteristics including grain structural changes in this severe plastic deformation layer using existing analytical means has not been successful [3].

In recent years, significant changes in the primary deformation zone were reported in various materials, including AISI stainless steel [4], iron [5], Inconel 718 alloy [6] and titanium [7]. While most of these studies on the

microstructure changes induced by machining were focus on the machined chips, there are few publications regarding the finished surface, which is more important than chips in most cases. To reveal the influence of continuous impact caused by cutting force to machined surface, a cutting experiment was conducted to discover the phase decomposition of alloy workpiece surface by using back-scattered electron microscopy [8-9]. The test results showed the structural transformation promotes the uncertainty of surface-topography. In addition, the grain structure changes in machined surface create the uncertainty of component performance. The effect of surface structure formation on workpiece life is not yet well understood since opposite treads still are obtained in literature. For instance, Schwach [10] found the component free of a metamorphic layer had a life six times that of a metamorphic layer component. As the white layer increases in thickness, the fatigue life decreases. In contrast, Ramesh [11] studied the residual stress induced by hard machining and found that it was significantly more compressive in the specimen with the white layer than that without it. Although existing researches tried to explain above contradictions, it is difficult to get a common point of view because of various experimental methods [12].

Recent years, the use of physics-based material models in FEM-based cutting models has received attention from scholars. Ding and Shin [13-14] researched the evolution of cell size during orthogonal cutting to model corresponding grain refinement. However, a key limitation of their mathematical models is that the grain size is just formulated as $d=K\rho_{tot}^{0.5}$ where $K$ is a constant and $\rho_{tot}$ is the total dislocation density, which implies that the grain evolution will occur even in the absence of dynamic recrystallize if the shear stress causes a net increase in $\rho_{tot}$. As one of mesoscale simulation methods, dislocation dynamics (DD) can provide new insights into some aspects of material behavior heretofore not explained using continuum approaches, such as dislocations structure changes, material strengthen mechanism, grain microstructure evolution. In particular, unlike fully discrete methods, such as molecular dynamic (MD), DD method offers better scalability to larger and more complex problem at the micrometer and sub-micrometer length scale. For instance, Shishvan [15] showed the simpler two-dimensional DDD studies are more successful in a range of applications encompassing microstructure evolution and plastic mechanism. Tarleton [16] adopted a planar discrete dislocation dynamic model to simulate micro-cantilever bending for hcp crystals oriented for plane strain prismatic slip. The results showed that pure bending interpretations of the micro-cantilever size effect do not reveal its full behavior and the inhomogeneous, highly localized stress influence the strengthening mechanisms and mechanical property. Liao [17] researched the interaction of dislocations and workpiece substrate structures during warm laser shock peening by multiscale discrete dislocation dynamics (MDDD). Their study showed that the impulse load facilitates the generation of highly dense and uniformly distribution structures and reinforces the surface strength of workpiece. The DD method provides a new means of researching the evolution of surface microstructure and mechanical property during micro-cutting process.

In this paper, the evolution of surface grain structure of titanium alloy under complex cutting conditions was studied through a two-dimensional climb assisted dislocation dynamic technology. The influence of crystal structure changes on the mechanical properties of machined surface was revealed. The paper is organized as follows: Section 2 gives a brief introduction to the coupling algorithm between finite element method and dislocation dynamic method. Section 3 presents the results and discussion. Finally, Section 4 ends the paper with some main conclusions.

## 2. Dislocation dynamic simulation framework for micro-cutting

### 2.1 Simulation algorithm of dislocation dynamics

In present study, a multi-scale simulation framework was developed by coupling the DD code into a finite-element package via python scripting. In this algorithm, the dislocation processes of generation, kinetics,

junction, immobilization, recovery, and annihilation were calculated by DD simulation. The finite element method (FEM) solver was used for the solution of applied stress of dislocations during micro-cutting process. In the presence of a large number of dislocations, the Peach-Koehler force on dislocation $I$ is written as

$$f_g^{(I)} = \left(\sigma + \sum_{J \neq I} \sigma_{ij}^{(J)}\right) b_j^{(I)} m_i \tag{1a}$$

$$f_c^{(I)} = -\left(\sigma + \sum_{J \neq I} \sigma_{ij}^{(J)}\right) b_j^{(I)} s_i \tag{1b}$$

Where $f_g^{(I)}$ is the dislocation slip force, $f_c^{(I)}$ is the dislocation climb force, $\sigma$ is the applied stress, $\sigma_{ij}$ denotes the internal resolved shear stress field induced by other dislocations, $b_j^{(I)}$ is Burger's vector of dislocation $I$ with unit normal $m_i$ and a unit vector $s_i$ in the slip direction [18].

The glide component of the Peach-Koehler (P-K) force on dislocation $I$ controls the glide velocity $v_g^{(I)}$ through the following drag law

$$v_g^{(I)} = M_g (f_g^{(I)} - f_0) \tag{2}$$

where $M_g$=1/$B_g$ and $M_g$ changes with temperature and pressure. $f_0$ is friction force. The dislocation climb is thermal activation movement and the dislocation climb velocity in the direction of $\boldsymbol{b}\times\boldsymbol{t}$ is

$$v_c = \frac{2\pi D_s v_a (F_e/L)}{b_e^2 kT} \tag{3}$$

where $D_s$ is self-diffusion coefficient, $v_\alpha$ is the vacancy volume and $b_e$ is magnitude of the Burgers vector, $c^0$ is vacancy partial equilibrium concentration of equilibrium state, $\sigma$ is dislocation climb P-K force, $k$ is the Boltzmann constant, $T$ is the absolute temperature [19-20].

Climbing is assumed to be governed by a drag-type relation similar to the dislocation slip with the help of nucleation and growth of dislocation jog. Dislocation climbs out the glide plane only if the climb distance is larger than the minimum distance between adjacent slip planes and the distance is equal to the magnitude of the Burgers vector. In particular, the time increment of dislocation climb is 100 times larger than that for glide [21-22]. In addition, they mutually block their movement if dislocations on inclined glide planes approach closely. Such locks form dislocation obstacles on their slip system against which subsequent dislocations will pile up. Nevertheless, upon stress reversal these locks will dissolve easily.

In DD framework, the nucleation event and close encounter of dislocations must be described by special rules. New dislocations are multiplied from the Frank-Read (F-R) sources, which have specific nucleation strength. The distribution density of F-R sources is in a random arrangement of crystal slip system. The nucleation time $t_{F\text{-}R}$ is defined as

$$t_{F-R} = \frac{\eta}{2} \frac{Bl}{\tau_{F-R} b} F(\xi) \tag{4}$$

where $\eta$ is 1.5, $\xi$ is $\tau/\tau_{\text{F-R}}$ and $F(\xi)$ is a rapidly decaying function. Avoiding all of dislocation sources are activated at the same time, the strength of each source is selected from Gaussian distribution randomly. The sign of new dislocation separates from each other, and the distance between the dislocation dipole must accord

$$L_{F-R} = \frac{G}{2\pi(1-\upsilon)} \frac{b}{\tau_{F-R}} \tag{5}$$

where $G$ is shear modulus, $v$ is Poisson's rate. Like the dislocation sources, the position of dislocation obstacles which can pin dislocation and subgrain boundary is also based on stochastic boundary in the slip system. In particular, the formation of a junction can either act as an obstacle or as a potential point for a F-R source is taken place when two dislocations gliding on two intersecting slip plane within a special distance [23]. Annihilation of two dislocations with opposite signed Burgers vectors occurs when they come within a critical annihilation distance 6$b$. This annihilation process is considered to be spontaneous and take place, even if the dislocations move on paralleled slip plane.

### 2.2 Trans-scale simulation model for micro-cutting

Commercial software Abaqus/Explicit was used to simulate the evolution of physical comprehension of surface microstructure and friction between the tool and the workpiece in micro-cutting of Titanium alloy. Fully coupled thermos-mechanical analysis was carried out for a time step of 0.5 ns to capture the applied stress of dislocations in each increment step. The resultant solution of unit increment was then imported to DD framework constantly, which treats plastic deformation as the evolution of a large number of dislocations. Since the calculation of long-range interactions among various dislocations brought an extremely computation burden, the DD simulation focuses on a representative cell in surface severe plastic deformation (SSPD) surface.

A 2D orthogonal cutting model was developed as shown in Fig.1. Linear quadrilateral continuum plane strain element with reduced integration was utilized for a coupled temperature-displacement analysis, and enhanced hourglass control was selected in this study for the entire set of elements [24]. The uncut chip thickness was 300 μm with uncut chip thickness being 40 μm. The single point diamond tool was built with a normal rank and flank angles of 15° and 6° respectively. The tool-cutting edge radius was 10 μm. The interaction of tool-workpiece was considered under dry aching conditions. The micro-cutting model was typically modeled by four geometrical parts to optimize the contact management, such as, Part1 - the insert active part, Part 2 - the uncut chip thickness, Part - 3 the tool-tip passage zone, and Part - 4 the workpiece support zone.

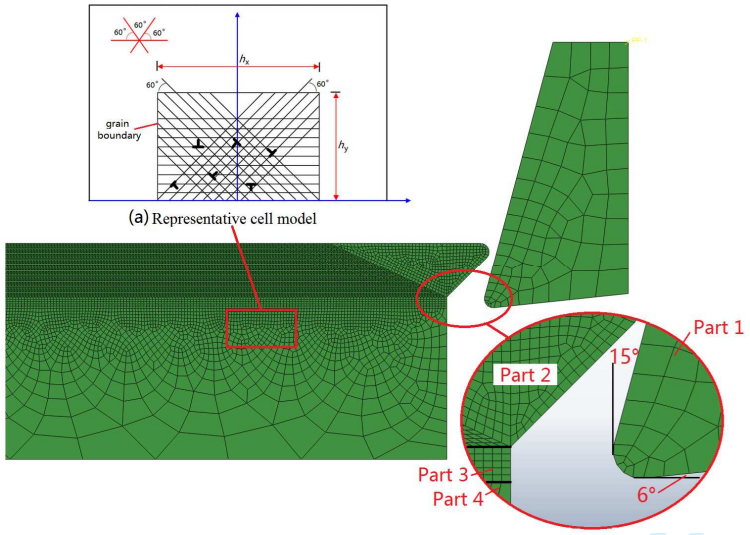


Fig.1 Dislocation dynamic simulation model of the micro-cutting of Titanium alloy (Ti-6Al-4V)

A two-dimensional representative cell model was built to perform the dislocation evolution in local area of workpiece surface as Fig.1 (a). Dislocations of titanium alloy moves in prismatic slip systems, with {1 0 -1 0} slip plane normal and [1 1 -2 0] slip direction [16]. The reference orientation for slip directions is (0, 60˚, 120˚) relative to the reference x-axis shown in Fig.1 (a). The $h_x/h_y$ of titanium alloy crystal of Ti-6Al-4V model for DD simulation of monotonic deformation is $2\sqrt{3}/3$. The pre-existing dislocation density $6.25\times10^{12}$ $m^{-2}$ and the dislocations are randomly placed on slip planes. The dislocation sources density is $4.2\times10^{13}$ $m^{-2}$. The cutting temperature *T is* 350K. As the impurity particles density of titanium alloy outclasses pure metal, the dislocation obstacle density is set to be $2.1\times10^{13}$ $m^{-2}$. The other material constants mimicking properties of Titanium alloy are list in Table 1.

Table.1 Material constants of titanium alloy Ti-6Al-4V

| Parameter | Value |
|---|---|
| Burgers vector ($b$) | 0.295nm |
| Shear modulus ($G$) | 113.76GPa |
| Poisson ratio ($v$) | 0.33 |
| Vacancy self-diffusion energy ($\Delta E_{sd}$) | 2.509eV |
| Pre-exponential diffusion constant ($D_0$ ) | 0.015 $cm^2/s$ |
| Gliding drag coefficient ($B_g$) | $1.4\times10^{-4}$ Pa s |
| P-N force ($f_0$) | 0.02MPa |
| Nucleation stress ($\tau_{nuc}$) | 0.8 GPa |

## 3. Results and discussion

### 3.1 Grain structure changes during micro-cutting process

Surface conditions and their modifications due to cutting-force play an important role in micro-cutting process. The complex dislocation motion and atomic migration result in the formation of cutting chip and rough machined surface. Fig. 3 shows the FEM-DD observations in the SSPD layer subjected to external load. Four typical deformation-induced microstructure features are identified as: dislocation line, dense dislocation band, subgrain boundary, and grain refinement. All analyses presented here are carried out using a static distribution of sources and obstacles as initial condition in Fig. 3 (a). A mass of dislocations are generated from the F-R sources when the stress meet or surpass the theoretical strength threshold of the material. In the initial stage of micro-cutting, the compression of cutting tool results in the compress at the tool-workpiece area and causes the mushrooming of dislocation at the cutting area. The combined interaction of compression stress and tensile stress drives the dislocations evolution. As the tool approached the representative cell, parallel dislocation lines are formed in the original grain in Fig. 3 (b). Meanwhile, grain hardening phenomena was induced by dislocation pile-up because the impenetrable lattice barriers blocked dislocation slip.

The micro manufacturing process is divided into two stages: the initial shock stage and dynamic recovery stage. In the former stage, various dislocation activities are normally motivated to accommodate plastic strain, including sliding, accumulation, interaction, and spatial rearrangement. It is shown that the distribution of dislocations is not uniform from Fig. 3 (c). The resolved shear stress of local area increases significantly with the decreasing of the distance between tool tip and the simulation cell. A growing number of dislocations take part in nucleating and extending. The tool-chip interface moved forward with the cutting tool, and the finished surface was formed during nano-cutting process. The dislocation density is pretty high in local region and high-density dislocation bands are formed by the non-equality dislocations distribution when tool tip arrived at the vertical area of cell. The dislocations are randomly arranged without preferable sliding orientations in early stage. Then, the cutting force prompts the microstructure and slide orientations to follow the feed speed direction, as Fig. 3 (c). In addition, the interaction of impenetrable dislocation bands and impurity particle produce pin-up strengthening. A mass of dislocations would encounter local obstacle such as stacking fault tetrahedral, defect clusters, junctions, which suppressed plastic deformation. According to Taylor relation [25], higher dislocation density around dislocation bands brings stress concentration, which also induces the surface grain to take place dislocation quadratic multiplication to release external load.

With the proceeding of cutting, the development of dislocation configurations gradually generates subdivision grain by forming individual dislocation cells. As shown in Fig. 3 (d), a shaped cell structure with a width of about half of original grain was obtained. This ‘boundary’ of cell was sharper and thinner than the dislocation band, but

the misorientations are more serious. The results indicated that dislocations annihilation and rearrangement transforms dislocation cells into independent subgrain structures in order to minimize the system energy of machined surface [26]. The increasing of dislocation density and inhomogeneous dislocation distribution resulted in the continuous refinement of surface grain. In addition, the simulation shows that refinement grain could not generate the dislocation lines and dislocation bands inside the subgrain if the size of stabilized grain is in submicron scale. This can be explained that the narrow crystal structure impedes the long range evolution of dislocations. Following, the finished surface takes place recovery process because of dislocation climb and annihilate. Since the dislocations migration and annihilate, vacancy defects are formed in the original location of dislocations. Then, the stacking fault energy of dislocations results in the continuous evolution of recrystallization, which leads to a gradually accumulation of boundary disorientation until the formation of high angle grain boundaries as Fig. 3 (e). The above observations are consistent with the previous experiment in Fig.3 [27], which indicates micro-cutting process not only offers a route for the manufacture of nanostructured titanium but also creates a surface with a refinement grain structure at the finished surface.

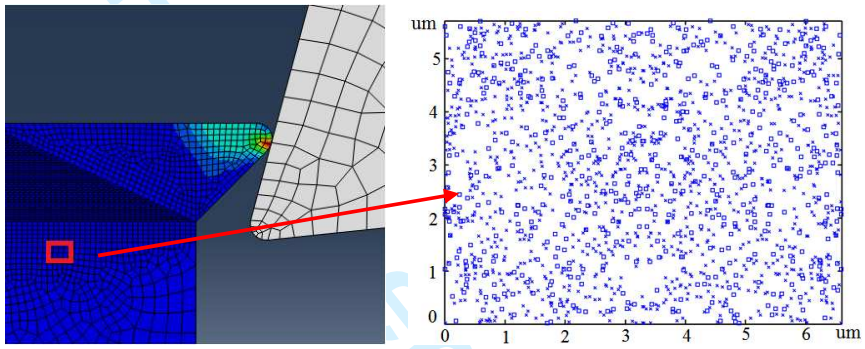


(a) The ‘o’ is pre-existing dislocation sources and ‘x’ is pre-existing dislocation obstacles before cutting

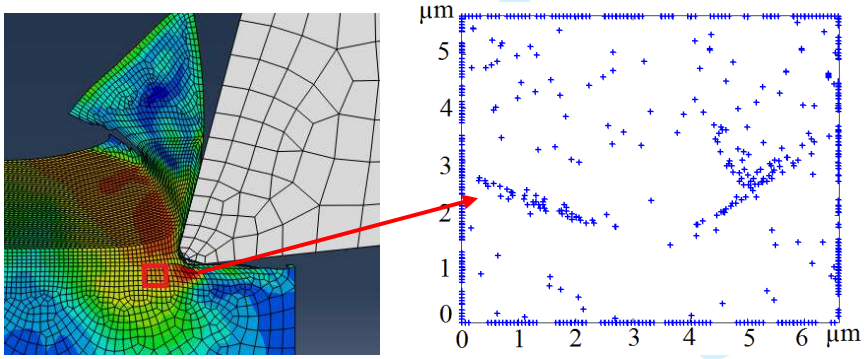


(b) Surface dislocation structure at 3000ns during cutting

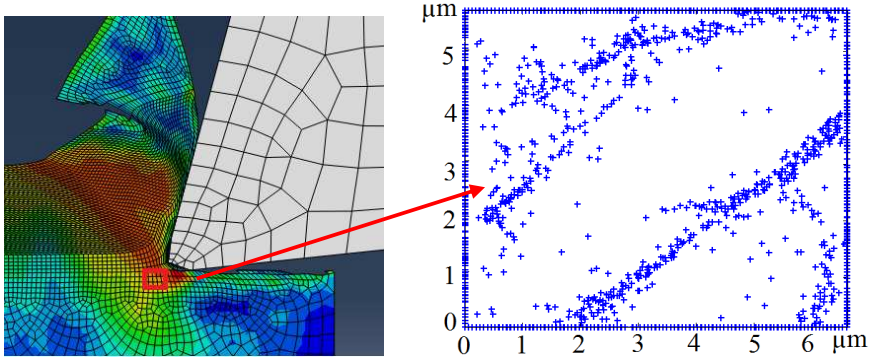


(c) Surface dislocation structure at 3500ns during cutting

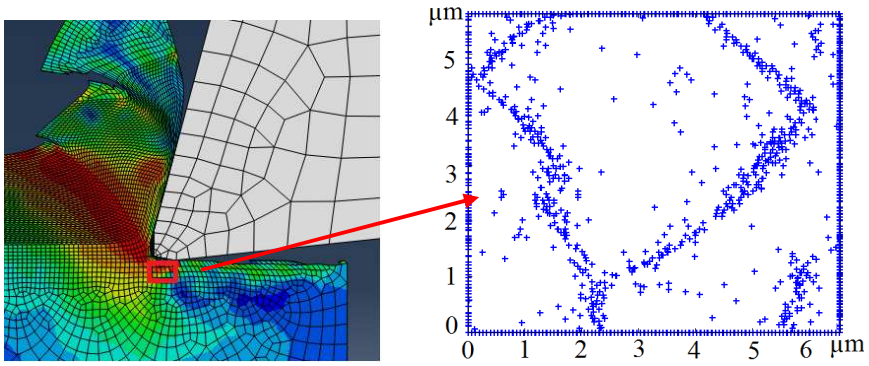


(d) Surface dislocation structure at 3750ns during cutting

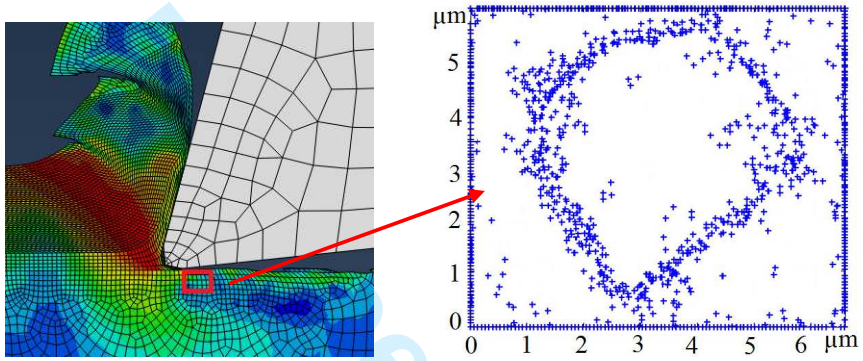


(e) Surface dislocation structure at 4000ns during cutting

Fig.2 Microstructure evolution of surface grain during micro-cutting process

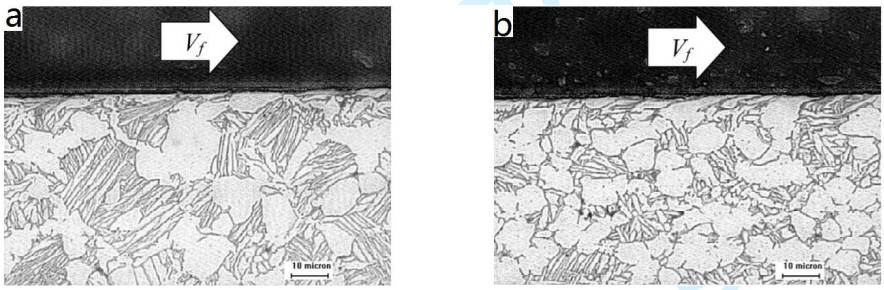


Fig.3 Microstructure alteration beneath the machined surface produced by Vc=100m/min, $f$=0.15 mm/tooth, $a_a$=2.0mm, $a_r$=8.8mm, and $V_f$ is feed speed direction: (a) initial cutting and (b) VB 0.3mm [27].

### 3.2 The effect of grain size on microscopic deformation field

From section 3.1, the cutting process promotes the evolution of microstructure in machined surface and grain refinement. In essence, according to the previous work [3], the change of grain structure directly results in an uncertainty of surface material property and affects severely machining quality. During cutting process, the most commonly method to reveal the interactive relation between surface properties and microstructure is Hall-Petch (H-P) equation [28-29]. However, models on size effect remains proportional to internal grain, which cannot obtain an accurate evolution mechanism of microscopic deformation field and mechanical properties of grain refining in most of studies [30]. A series of experiments and simulations indicated that the size effect of surface and chip grain structure brings some uncertainties in H-P exponent $q$, which always leads to contradictory conclusions [31]. For instance, the $q$ is rough 0.5 without considering the effect of work hardening in micro-cutting process [32-33]. In

order to reveal the plastic behavior of grain structure changes and study on the vagueness of surface mechanical property, a confining $h_x$=13.2 μm and a range of crystal lattice number n={2×2, 4×4, 8×8, 20×20} is shown in Fig.4.

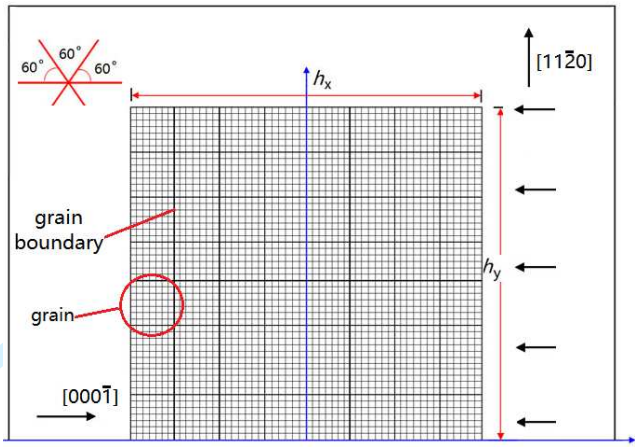


Fig.4 Sketch of the boundary value problem with various grain structure

To obtain internal stress responses and stress-strain curves of workpiece finished surface, the relaxed configurations were subjected to an external stress. Then it could generate dislocations and produce plastic strain. Specifically, the strain rate was constantly monitored to exclude the influence of high strain rate in this simulation [34]. The plastic strain rate at any time and region can be calculated by

$$\dot{\gamma}_p = \phi b \rho \frac{d\bar{l}}{dt} + \phi b \bar{l} \frac{d\rho}{dt} \tag{6}$$

where $\phi$ is correction factor, $\rho$ is density of mobile dislocation, $b$ is Burgers vector, $\bar{v}$ is average speed of dislocation, and $\bar{l}$ is mean distance traveled by a dislocation in an increment step. When the plastic strain rate permanently is blows 10 $s^{-1}$ the simulation domain is considered as being relaxed and the plastic strain is attributed to the applied stress. The local distribution pattern of dislocation microstructure and internal stress states for various lattice sizes are shown as Fig.6.

In present study, the pre-existing dislocations of initial configurations were used to study the plastic behavior. To perform size effect simulations over time durations sufficient to establish a steady state, an adaptive scheme was used to increment the simulation time step proceeding. The initial unrelaxed configuration is achieved by distributing the special density of dislocations randomly, as the Fig.5 (a). Then the dislocations are relaxed at zeros stress until the dislocations attained quasi-equilibrium position. The representative cell is subdivided into hexagonal grains of equal size and grain boundaries are impenetrable barriers. The microscopic deformation fields and internal stress with various grain sizes are shown in Fig.5. During the micro-cutting process, the structure evolution of dislocations pattern develops from simpleness to complexity. A large number of dislocations encounter nano-precipitates and junctions, which interacts with dislocations at short ranges and influences local dislocation pattern. The energy aggregation caused by residual stress facilitates dislocations nucleation and forms continuous slip bands span multiple grains. However, Fig.6 shows how grain boundaries act as barriers in plastic deformation. The boundaries prevent dislocations moving from one grain to neighboring. Therefore, the number of restricted dislocations increases with the decline of mean lattice size. A mass of dislocations pile up in the grain boundary can induce surface hardening phenomenon.

According to the distribution of residual stress, both stress nephogram and ribbon have fully verified the exactness of above analysis. Almost all of stress concentration regions (SCR) focus on grain boundaries. This

observation falls within theoretical expectations that dislocations microstructure contains a hard grain boundaries with high local dislocation density and a soft grain regions with low dislocation density [35-36]. From Fig. 5 (b-d), increasing stress difference has been shown at the upper or lower end of histogram. The stress fields shown in different micrographs indicate that the inner stress becomes increasingly polarized. This is due to the increasing of dislocation density with plastic strain and the high concentrations of dislocations at grain boundaries. The extreme stress drives the deformation and distortion of grain boundary and induces the aberrance of crystal lattice. Hence the squash and stretch near lattice boundary greatly reduces the fatigue life of titanium alloy and causes the initiation and evolution of micro-crack. However, the above facts are significantly reduced and the stress gradients within lattice also become more obscure once the grain size drops below 1.65 μm (as shown in Fig.5 (f)). Although the area of stress concentration region increased, the influence of stress concentration reduces greatly. The refinement brings the quantity of grain boundary increases exponentially and eases the cumulative effect of dislocation pile-up. Therefore, the dislocations more easily arrive at grain boundaries and then absorbed in small grain. However, the back stress induced by grain boundary pile-up also makes it harder to reactivate the sources from the slip plane where the dislocations originated. This phenomenon causes hardening and eventually leads to the nucleation of dislocations on neighboring slip planes that under a state of lower resolved shear stress.

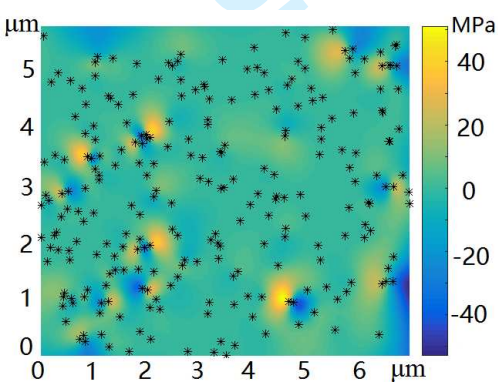


(a) Unrelaxed configurations of pre-existing dislocation

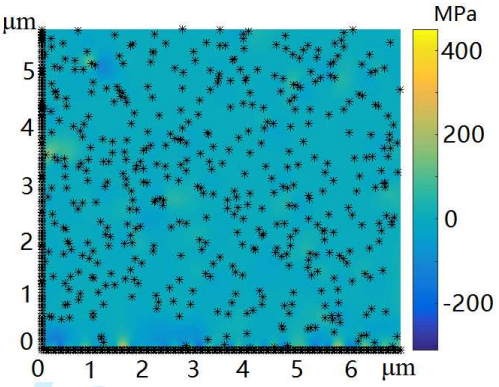


(b) Gain number is 1×1 and grain size is 13.2μm×11.44μm

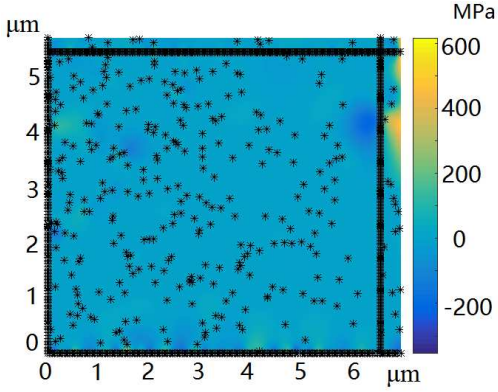


(c) Grain number is 2×2 and grain size is 6.6μm×5.72μm

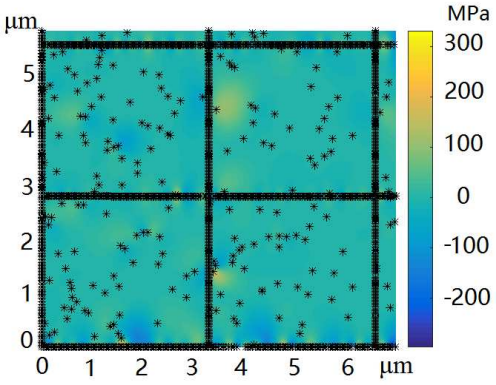


(d) Grain number is 4×4 and grain size is 3.3μm×2.86μm

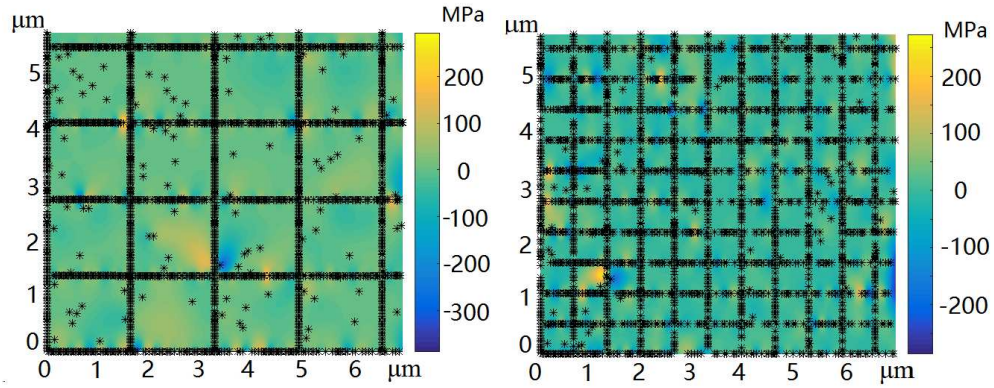


(e) Grain number is 8×8 and grain size is 1.65μm×1.43μm (f) Grain number is 20×20 and grain size is 0.66μm×0.572μm

Fig.5 Local distribution of $\sigma_{xx}$ and dislocations of titanium alloy (Ti-6Al-4V)

### 3.3 The effect of grain size on dislocation evolution and stress-strain response

As the dislocation density on boundaries is several decouples higher than other regions, the mean dislocation density can be calculated as Eq.7

$$\overline{\rho} = \varphi\rho_w + (1-\varphi)\rho_c \tag{7}$$

where $\overline{\rho}$ is mean dislocation density, $p_w$ is the dislocation density of grains boundaries, and $p_c$ is the dislocation density of inner lattice. In this equal, $\varphi$ is volume fraction of cell walls and it is 0.2 here. In order to reveal the evolution dislocation density with various mean lattice sizes, the various curves of dislocation density versus plastic strain or time are modeled by classical theory as in Fig.6.

The different microstructure results in various dislocations movement loci, which determines dislocation mobility. As shown in Fig.6 (a), the evolution curves of nucleation dislocation density are mutual consistency in small stain. Then matrix takes place different levels of dislocation multiplication with the increasing of strain. The slope of curve for $d_x$=0.66 μm is much higher than others, indicating the nucleation rate is the fastest in submicron grain. Since the dislocation moves only in a limited distance in ultra-fine grain, the plastic deformation of titanium alloy is small, and this drives the proliferation of dislocations to release the external load. The mean dislocation density (as Fig.6 (b)) declines in initial period as the influence of obstacles and annihilate. In particular, these curves appear an obvious turning point halfway, which marks that the resolved shear stress is large enough to activate dislocation dipole. Then, the entangled of curves disappears and a clear distinction occurs along with time. Likewise, the quality of movable dislocations gradually declines and bottoms out originally as Fig.6 (c). Specifically, the curve of $d_x$=0.66μm firstly rebounds. It can be explained that mobile dislocation density in refine grain decreases rapidly and then causes the dislocation starvation effects [37]. Dislocations leave the crystal more quickly than they multiply and leading to the requirement of continual dislocation nucleation in the course of plastic deformation. In particular, the grain refinement shows significant activity to promote the proliferation of dislocation, which induces the weakness nucleation of titanium alloy grain in subsequent deformation, leading to the structure hardening. This conclusion is consistent with dislocations pattern shown in Fig. 5.

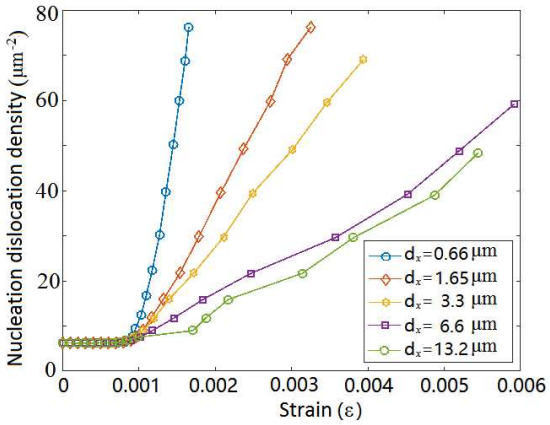


(a) The dislocation density versus strain

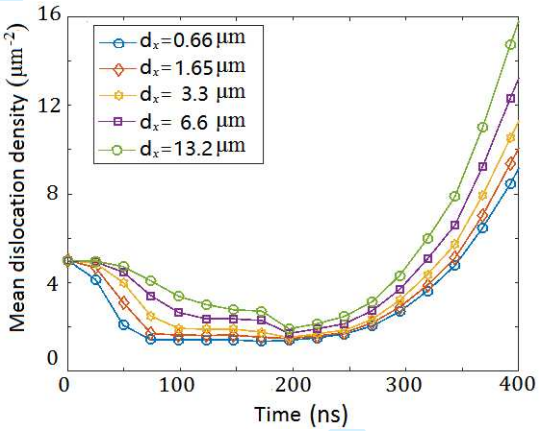


(b) The mean dislocation density versus with time

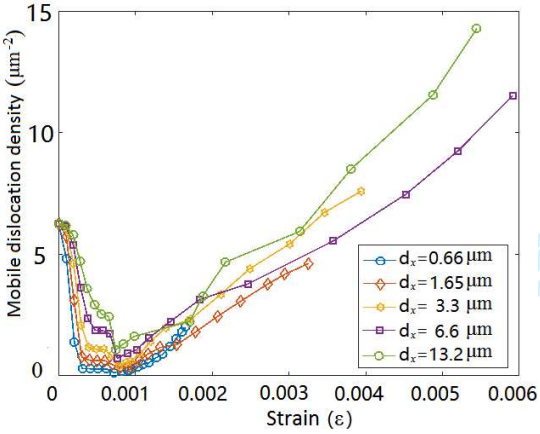


(c) The mobile dislocation density with stain

Fig.6 The dislocation density of titanium alloy (Ti-6Al-4V) evolutions with various mean lattice sizes

Constitutive laws describe the relation among macroscopic quantities such as stress, strain, and strain rate [38]. Most of the constitutive laws reported can be attributed to the group of local models in which the total deformation gradient has been decomposed into elastic and plastic parts multiplicatively [39-40]. However, if the grain scale is too smaller, the local model will be insufficient owing to its inability to describe the size effects. The multiplication and constraint of dislocations are related to the curvature of plastic deformation and the effective plastic strain gradient. To further investigate the influence of grain refinement on the mechanical property of workpiece surface,

Fig.7 shows the computationally obtained stress-strain curves by considering dislocation climb for selected grain sizes. The same pre-existing dislocation density, dislocation sources density, dislocation obstacles density and spatial distribution are assigned for all these cases.

As shown in Fig.7, the initial slope of stress-strain curves for random dislocation configured domains of different grain size depends on the grain sizes at larger strain plastic strain. Workpiece hardening is more pronounced in small domain. As shown in Fig. 7 (a), there is a nearly ideally plastic response when grain sizes $d_x$ is equal or larger than 6.6 μm. However, the smaller grain polycrystals have an increased hardening rate because the crystal boundary of fine grain inhibits the slip length of independent dislocation and limits the density of mobile dislocation. These lead to the dislocations not to form sufficiently slip bands that span many grains. Meanwhile, coarse grain reduces the effectiveness of the grain boundaries as barriers, which can inherently form the slip band to release the external stress. Therefore, the propagation and blocking of dislocations evolution primarily induces the grain size dependence rather than the incompatible caused by twist boundary during refinement process. However, it is dramatic that the stress-strain curve has a completely opposite evolution process in small strain stage as shown in Fig. 7 (b). In addition, there is always a sharp transition in the work hardening rate between small-scale plasticity and large-scale plastic yielding. The reason is that dislocation configurations in large grain usually have far more complex microstructure at zero applied stress relax by forming dipoles or lacks. Therefore small grain dislocations are more easily detach from the dipoles.

As shown in Fig.7 (a), the flow stress and hardening rate are both decreased for all of grain sizes when the dislocation-climbing is taken into account. Meanwhile, a perfect soften effect has been captured when climb is considered for the polycrystals with a grain size $d_x \geq 1.65$μm. In particular, this is an inverse effect when the mean grain size dx $\leq$ 1.65μm. The opposite phenomenon causes the uncertainty of surface-topography which is described in the introduction. It can be explained the subsurface temperature which is slightly above ambient could enhance dislocation glide and climb by altering the dislocation drag, but it is insufficient to improve the ability of absorbing and transmitting dislocations at boundaries. Therefore, although dislocation climb can promote dislocations to jump out of a special slip plane to elude the dislocation obstacles, it also helps the dislocation absorption rate by flank both impenetrability edges.

The evolution of yield strength with grain size is presented in Fig.7 (c). The stress at strain $\varepsilon_P$=0.2% is defined as the yield stress. Once the dislocation climb has been considered, the yield stress drops sharply with the decreasing of grain size. This verifies our original inference that although the H-P relation is useful for grain size effect, the important parameter in this equal has been permanently changed by the complex cutting environment. For different grain sizes, the simulation results are repeated to calculate the yield stress induced by random distributions of F-R sources. It can be clearly seen that the DD simulation results can be well described by the H-P relation as eq. (8), i.e. the yield stress increases with decreasing grain size.

$$\tau = \tau_0 + kd^{-q} \tag{8}$$

where $\tau_0$ is yield stress with sufficiently large grain size, $k$ is material-specific coefficient, and $q$ is sensitivity exponent of grain size. Although both slope $k$ and exponent $q$ depict the grain size effect, the power exponent $q$ is a more dominant parameter. The best fit equations are shown in Fig. 7 (c), parameter $\tau_0$ is 488.4 MPa for the case with dislocation climb considered and the value of $q$ is 1.297. Such a value seems surprisingly high, but it falls within a series of investigations. For instance, Evers [41] obtained the value of q in the range 1.19 to 1.5 by using a scale dependent model to predict grain size effects under plane stress loading condition. For polycrystals with grain sizes in the range of several microns, various simulations both predict the same high value q is 1-1.5 [16, 42]. In fact, yield strength is only sensitive to grain size for a sufficiently large grain. However to smaller grain, the grain size, obstacle density and the details of grain crystallography has determined the exponent.

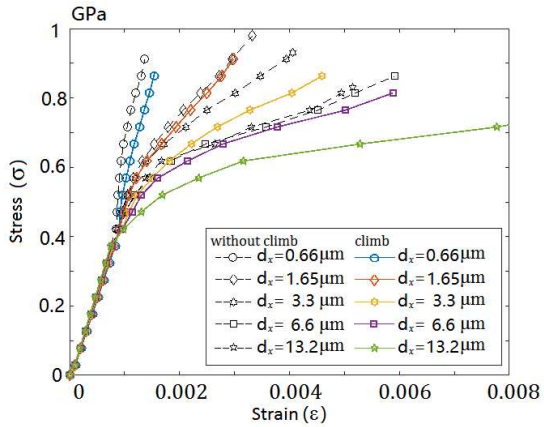


(a) Stress-strain curve for different grain size

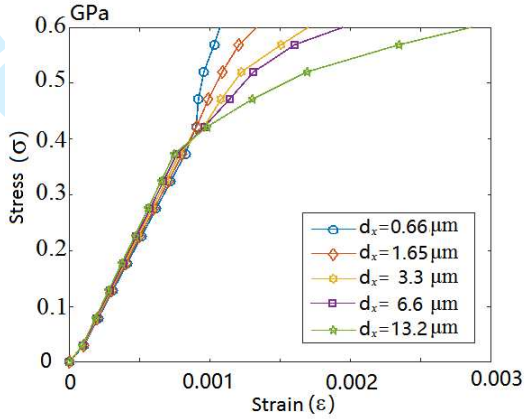


(b) Local enlargement of figure (a) to show the behavior at small strain

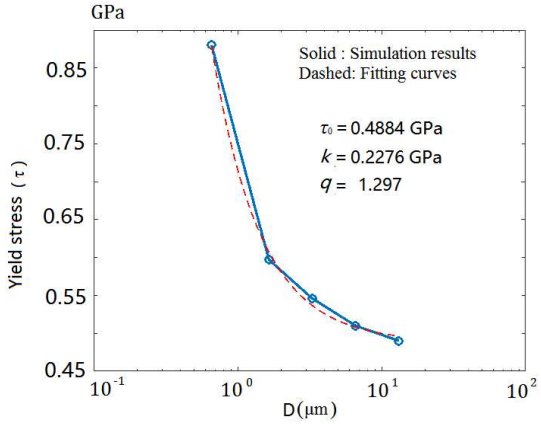


(c) Grain size dependence of yield strength

Fig.7 Quasi-static stress-strain curves of titanium alloy (Ti-6Al-4V) with selected grain sizes $d_x$={0.66, 1.65, 3.3, 6.6, 13.2} μm

## 4. Conclusions

In this study, the micro-cutting of titanium alloy was stimulated by climb assisted dislocation dynamic method. A special focus was given to the dependency between grain structure and mechanical properties of finished surface. The conclusions are list as following:

(a) The predications of simulation fall within the previous experimental ranges, which demonstrated the feasibility of using the proposed two-dimensional mesoscale analysis method to study the surface

microstructure evolution during micro-cutting process.

(b) A cutting induced surface grain refinement process is found in micro-cutting of titanium alloy. The process can be described as follows: the development of dislocation lines in original grains, the formation of dense dislocation bands, the transformation of dislocation bands into subgrain boundaries, and the continuous dynamic recrystallization in subgrain boundaries.

(c) The grain boundary and PSB in surface bring appreciable scale effect by preventing dislocations moving from one to neighboring grain. In addition, nearly all of SCRs gather around the grain boundaries of Ti-6Al-4V, which can induce the crystal distortion and aberrance.

(d) With dislocation climb considered, the flow stress and hardening rate are both sharply decreased. Dislocation climb significantly weakens the grain size effect of workpiece surface grain with several microns sized grains. However, it has an opposite effect of polycrystals with submicron sized grains in micro-machining.

(e) Based on a bottom-up approach, the Hall-Petch type scaling of yield strength with grain size has been calculations, q=1.297, in various grain size. This result can actually reveals the interactive relationship between grain size and mechanical property for Ti-6Al-4V.

## Acknowledgments

This research work was jointly supported by the National Natural Science Foundation of China (Grant No. 51575138) and the State Key Program of National Natural Science Foundation of China (Grant No. 51535003).

## Reference

[1] D. Ulutan, T. Ozel. Machining induced surface integrity in titanium and nickel alloys: A review. International Journal of Machine Tools & Manufacture. 2011, 51: 250-280.

[2] R. M'Saoubi, J.C. Outeiro, H. Chandrasekaran, et al. A review of surface integrity in machining and its impact on functional performance and life of machined products. International Journal of Sustainable Manufacturing. 2008, 1(1-2): 203-236.

[3] I. S. Jawahir, E. Brinksmeier, R. M'Saoubi, et al. Surface integrity in material remove process: recent advances. CIRP Annals- Manufacturing Technology. 2011, 60: 603-626.

[4] E. Brinksmeier, R. Gläbe, J. Osmer. Ultra-precision diamond cutting of steel molds. CIRP Annals-Manufacturing Technology. 2006, 55(1): 551-554.

[5] S. Swaminathan, M. R. Shankar, S. Lee, et al. Large strain deformation and ultra-fine grained materials by machining. Materials Science and Engineering A. 2005, 410-411: 358-363.

[6] M. A. Hadi, J. A. Ghani, C. H. Haron. Effect of cutting speed on the carbide cutting tool in milling Inconel 718 alloy. Journal of Materials Research. 2016, 31(13): 1885-1892.

[7] M. R. Shankar, S. Lee, S. Chandrasekhar. Severe plastic deformation (SPD) of titanium at near-ambient temperature. Acta Materialia. 2006, 54: 3691-3700.

[8] S. Wang, S. To, C. Y. Chan, et al. A study of the cutting-induced heating effect on the machined surface in ultra-precision raster milling of 6061 Al alloy. International Journal of Advance Manufacture Technology. 2010, 51(1-4): 69-78.

[9] S. J. Zhang, S. To, C. F. Cheung, et al. Micro-structural changes of aluminum alloy influencing micro-topographical surface in micro-cutting. International Journal of Advanced Manufacturing Technology. 2014, 72: 9-15.

[10] D. W. Schwach, Y. B. Guo. A fundamental study on the impact of surface integrity by hard turning on rolling contact fatigue. International Journal of Fatigue. 2006, 28: 1838-1844.

[11] A. Ramesh, S. N. Melkote, L.F. Allard, et al. Analysis of white layers formed in hard turning of 52100 steels. Materials Science and Engineering A. 2005, 390: 88-97.

[12] V. M. Fedirko, O. H. Luk'Yanenko, V. S. Trush. Influence of the diffusion saturation with oxygen on the durability and long-term static strength of titanium alloys. Materials Science. 2014, 50(3): 415-420.

[13] H. T. Ding, Y. C. Shin. Dislocation density-based grain refinement modeling of orthogonal cutting of commercially pure Titanium. In: Proceedings of the 2011 ASME International Manufacturing Science and Engineering Conference, MSEC2011-50220, Corvallis, OR, USA, 2011, p. 10.

[14] H. T. Ding, Y. C. Shin. Multi-physics modeling and simulations of surface microstructure alteration in hard turning. Journal of Materials Processing Technology. 2013, 213: 877–886.

[15] S. S. Shishvan, E. Van der Giessen. Mode I crack analysis in single crystals with anisotropic discrete dislocation plasticity: I. formation and crack growth. Modelling and Simulation in Materials Science and Engineering. 2013, 21(065006): 1-21.

[16] E. Tarleton, D. S. Balint, J. Gong et al. A discrete dislocation plasticity study of the micro-cantilever size effect. Acta Materialia. 2015, 88: 271-282.

[17] Y. L. Liao, Y. Chang, H. Gao, et al. Dislocation pinning effects induced by nano-precipitates during warm laser shock peening: dislocation dynamic simulation and experiments. Journal of apply physics. 2011, 110(023518): 1-7.

[18] Van der Giessen, E. Needleman. Discrete dislocation plasticity: a simple planar model. Modelling and Simulation in Materials Science and Engineering. 1995, 3:689-735.

[19] M. S. Huang, Z. H. Li, J. Tong. The influence of dislocation climb on the mechanical behavior of polycrystals and grain size effect at elevated temperature. International Journal of Plasticity. 2014, 64: 112-127.

[20] K. Danas, V. S. Deshpande. Plane-strain discrete dislocation plasticity with climb-assisted glide motion of dislocations. Modelling and Simulation in Materials Science and Engineering. 2013(21):045008.

[21] C. Ayas, V. S. Deshpande, M. G. D. Geers. Tensile response of passivated films with climb-assisted dislocation glide. Journal of the Mechanics and Physics of Solids. 2012, 60(9): 1626-1643.

[22] K. M. Davoudi, L. Nicola, J.J. Vlassak. Dislocation climb in two-dimensional discrete dislocation dynamics. Journal of Applied Physics. 2012, 111(10): 103522-103522-7.

[23] A. A. Benzerga, Y. Brechet, A. Needleman, et al. Incorporating three-dimensional mechanisms into two-dimension dislocation dynamics. Modelling and Simulation in Materials Science and Engineering. 2004, 12:159-196.

[24] Y. C. Zhang, T. Mabrouki, D. Nelias, et al. Chip formation in orthogonal cutting considering interface limiting shear stress and damage evolution based on fracture energy approach. Finite Elements in Analysis and Design. 2011, 47: 850-863.

[25] R. K. Al-Rub, G. Z. Voyiadjis. A physical based gradient plasticity theory. International Journal of Plasticity. 2006, 22: 654-684.

[26] N. R. Tao, Z. B. Wang, W. P. Tong, et al. An investigation of surface nanocrystallization mechanism in Fe induced by surface mechanical attrition treatment. Acta Materialia. 2002, 50: 4603-4616.

[27] A. Ginting, M. Nouari. Surface integrity of dry machined titanium alloys. International Journal of Machine Tools & Manufacture. 2009, 49: 325-332.

[28] G. D. Hughes, S. D. Smith, C. S. Pande, et al. Hall-petch strengthening for the micro hardness of twelve nanometer grain diameter electrodeposited Nickel. Scripta Metallurgica. 1986, 20: 93–97.

[29] R. Liu, M. Salahshoor, S. N. Melkote. A unified material model including dislocation drag and its application to simulation of orthogonal cutting of OFHC Copper. Journal of Materials Processing Technology. 2015, 216:

328-338.

[30] N. Ahmed, A. Hartmaier. Mechanisms of grain boundary softening and strain-rate sensitivity in deformation of ultrafine-grained metals at high temperatures. Acta Materialia. 2011, 59: 4323-4334.

[31] Z. H. Li, C. T. Hou, M. S. Huang, et al. Strengthening mechanism in micro-polycrystals with penetrable grain boundaries by discrete dislocation dynamics simulation and Hall-Petch effect. Computational Materials Science. 2009, 46: 1124-1134.

[32] Q. Q. Wang, Z. Q. Liu, B. Wang. Evolutions of grain size and micro-hardness during chip formation and machined surface generation for Ti-6Al-4V in high-speed machining. International Journal of Advance Manufacture Technology. 2016, 82: 1725-1736.

[33] G. Rotella, D. Umbrello. Finite element modeling of microstructural changes in dry and cryogenic cutting of Ti6Al4V alloy. CIRP Annals- Manufacturing Technology. 2014, 63:1–4.

[34] N. Ahmed, A. Hartmaier. A two-dimensional dislocation dynamics model of the plastic deformation of polycrystalline metals. Journal of Mechanics and Physics of Solids. 2010, 58: 2054-2064.

[35] R. Sedlacek. Internal stresses in dislocation wall structures. Scripta Metallurgica. 1995, 33(2): 283-288.

[36] J. S. Kim, J. H. Kim, Y. T. Lee. Microstructural analysis on boundary sliding and its accommodation mode during superplastic deformation of Ti-6Al-4V alloy. Materials Science and Engineering: A. 1999, 263: 272-280.

[37] W. D. Nix, J. R. Greer, G. Feng, et al. Deformation at the nanometer and micrometer length scales: Effects of strain gradients and dislocation starvation. Thin Solid Films. 2007, 515: 3152-3157.

[38] H Katsuragi. Constitutive laws. Volumes 3, Springer, Japan, (2016).

[39] G. Z. Quan, G. C. Luo, J. T. Liang, et al. Modelling for the dynamic recrystallization evolution of Ti-6Al-4V alloy in two-phase temperature range and a wide strain rate range. Computational Materials Science. 2015, 97:136-147.

[40] G. Chen, C. Z. Ren, X. Y. Yang, et al. Finite element simulation of high-speed machining of titanium alloy (Ti-6Al-4V) based on ductile failure model. International journal of Advance Manufacture Technology. 2011, 56:1027-1038.

[41] L. P. Evers. W. A. M. Brekelmans. M. G. D. Geers. Scale dependent crystal plasticity framework with dislocation density and grain boundary effects. International Journal of Solid and Structure. 2004, 41: 5209-5230.

[42] U. Borg. A strain gradient crystal plasticity analysis of grain size effects in polycrystals. European Journal of Mechanics A/Solids. 2007, 26(2): 313-324.